Effect of pellet fuelling on energy transport in ohmically heated alcator C plasmas

EFFECT OF PELLET FUELLING ON ENERGY TRANSPORT IN OHMICALLY HEATED ALCATOR C PLASMAS

S.M. WOLFE, M. GREENWALD, R. GANDY*,
R. GRANETZ, C. GOMEZ, D. GWINN, B. LIPSCHULTZ,
S. McCOOL**, E. MARMAR, J. PARKER***,
R.R. PARKER, J. RICE
Plasma Fusion Center,
Massachusetts Institute of Technology,
Cambridge, Massachusetts,
United States of America

ABSTRACT. Time-dependent transport analysis calculations have been carried out, using experimentally determined plasma parameters to obtain the variation of electron and ion thermal diffusivities following pellet injection into moderate-density Alcator C discharges. The ion thermal diffusivity, which is typically higher than neoclassical predictions by a factor of three to five in the gas-fuelled target plasma, is found to decrease after pellet injection to approximately the neoclassical value. The electron thermal conductivity is not reduced after pellet injection. The improvement in ion transport correlates with the peaking of the density profile and may be related to the reduction in the quantity $\eta_i \equiv d \ln T_i / d \ln n$, which is inferred to lie close to the critical value for stability of drift modes driven by the ion temperature gradient. Extrapolation of these results to higher-density plasmas, for which the electron and ion losses cannot be unambiguously measured, is consistent with previously reported increases in global energy confinement time accompanying pellet injection.

1. BACKGROUND AND MOTIVATION

Pellet fuelling has been demonstrated [1] to result in improved global energy confinement in high-density ($\bar{n}_e > 3 \times 10^{20} m^{-3}$) ohmically heated plasmas in the Alcator C tokamak. This range of densities corresponds, for gas-fuelled discharges, to the 'saturated confinement regime' [2, 3], in which energy confinement departs from the neo-Alcator [2–4] scaling $\tau_E \propto \bar{n}_e R^{2.04} a^{1.04}$, which holds for lower density. With pellet fuelling, no degradation in confinement relative to the empirical scaling is observed for densities $\bar{n}_e \leqslant 5 \times 10^{20} m^{-3}$. At the highest densities, $5 \times 10^{20} < \bar{n}_e < 1 \times 10^{21} m^{-3}$, the pellet-fuelled discharges have confinement times consistent with neoclassical ion transport and values of the confinement parameter, $n_0 \tau_E$, in excess of the Lawson criterion for thermalized breakeven.

Neither the relatively poor confinement in gas-fuelled discharges nor the improved performance with pellet injection has been satisfactorily explained. In particular, since at high density the electron and ion temperatures are closely coupled, it is not possible to determine unambiguously whether the improvement relative to gas-fuelled discharges is due to reductions in electron losses or ion losses. Previous experiments in gas-fuelled discharges at lower density indicated the presence of anomalous ion thermal conduction loss [2–4]. An ion thermal diffusivity, χ_i, roughly three to five times greater than the Chang–Hinton neoclassical prediction [5] was inferred from those results. Such an anomaly would be sufficient to account for the observed confinement behaviour in higher-density gas-fuelled plasmas. Moreover, the nominal values of $(T_e - T_i)$ in these discharges are consistent with such an anomalous ion loss [3]. It is therefore natural to suppose that the beneficial effect of pellet injection is due to suppression of anomalous losses through the ion channel, perhaps through modification of the density or pressure profile.

However, the data for the high-density gas-fuelled plasmas are also consistent, within the experimental uncertainty, with increased electron thermal conductivity, relative to the neo-Alcator value. This alternative interpretation [6] of the confinement 'saturation'

---

* Present address: Department of Physics, Auburn University, Auburn, AL, USA.
** Present address: Fusion Research Center, University of Texas, Austin, TX, USA.
*** Present address: Advanced Technology Engineering, Varian, Beverly, MA, USA.

suggests an analogy to the appearance of enhanced electron losses in L-mode neutral-beam-heated tokamaks. The improved confinement in pellet-fuelled discharges might then be interpreted as a transition to the H-mode resulting in a decrease in electron thermal conductivity.

In order to ascertain the power flow in an Ohmic discharge, it is necessary to determine the power, $P_\Delta \propto n^2 T_e^{3/2}(T_e - T_i)$, corresponding to electron–ion coupling. To clarify the effect of pellet injection on electron and ion heat transport processes, we have carried out pellet injection experiments at moderate density ($1 \times 10^{20} < \bar{n}_e < 3 \times 10^{20}\,m^{-3}$); for these parameters, T_e and T_i are sufficiently separated relative to their experimental uncertainties for the electron and ion energy loss channels to be distinguished. Global energy confinement times in these plasmas are typically in the 'unsaturated' or electron-dominated regime characterized by neo-Alcator scaling. We employ time-dependent transport analyses using the experimentally determined plasma parameters to obtain the variation of electron and ion thermal diffusivities during these discharges.

2. EXPERIMENT

In the present experiments, the Alcator C tokamak (major radius R = 0.64 m, minor radius a = 0.165 m) was operated at toroidal fields in the range $8.0 \leqslant B_T \leqslant 10.0$ T, with plasma current $250 \leqslant I_p \leqslant 550$ kA. Frozen deuterium pellets were injected at about 600–800 $m \cdot s^{-1}$ into ohmically heated D^+ discharges by means of a four-shot pneumatic injector [7]. Two pellet sizes, with diameters of 1.0 and 1.5 mm, containing approximately 3×10^{19} and 6×10^{19} deuterium atoms respectively, were employed. The density of the target plasma was typically in the range $1 < \bar{n}_e < 2.5 \times 10^{20}\,m^{-3}$. Molybdenum limiters were employed throughout the course of these experiments.

Plasma current and one-turn voltage were monitored by standard magnetic diagnostics. Electron temperature profiles, $T_e(r, t)$, were obtained from second-harmonic electron cyclotron emission (ECE) using scanning Fabry-Perot and grating instruments. Absolute calibration was derived from Thomson scattering and soft-X-ray pulse-height analysis. The density profiles were measured using a five-chord FIR laser interferometer; single time points were also obtained from Thomson scattering. Measurement of visible bremsstrahlung emission provided information on Z_{eff} and supplemented the density profile data. The (d, d) neutron rate, which is sensitive primarily to the central ion temperature, was determined from calibrated BF_3 long counters and a bank of He^3 detectors.

Figure 1 depicts a typical pellet injection shot. A single pellet is injected at about 310 ms, raising the line-average density by approximately $1.2 \times 10^{20}\,m^{-3}$. As the plasma is diluted by cold particles from the pellet, the electron and ion temperatures decrease, leading to a drop in neutron rate and an increase in the resistive voltage. There is also a small decrease in total plasma current. On the fast time-scale ($\leqslant 1$ ms) the total kinetic energy of the plasma is essentially unchanged. The plasma then re-heats in about 40 ms,

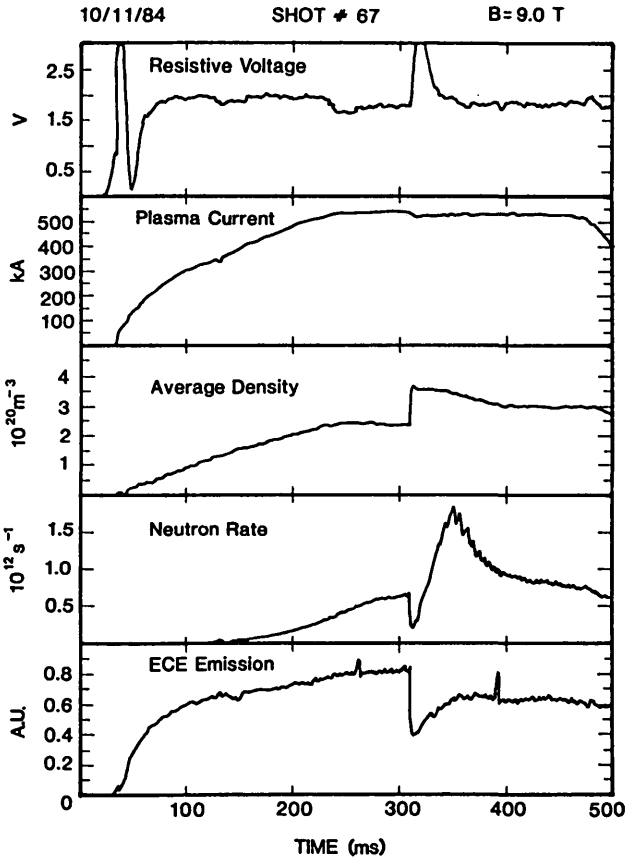

FIG. 1. Variation of plasma parameters during a typical pellet injection shot. The resistive voltage is obtained from the measured surface voltage by accounting for the change in magnetic energy using a simple model of the current density profile. Line-average density is measured by the central chord of a FIR interferometer. Second harmonic electron cyclotron emission from the plasma centre is proportional to the central electron temperature. The deuterium pellet is injected at approximately 310 ms.

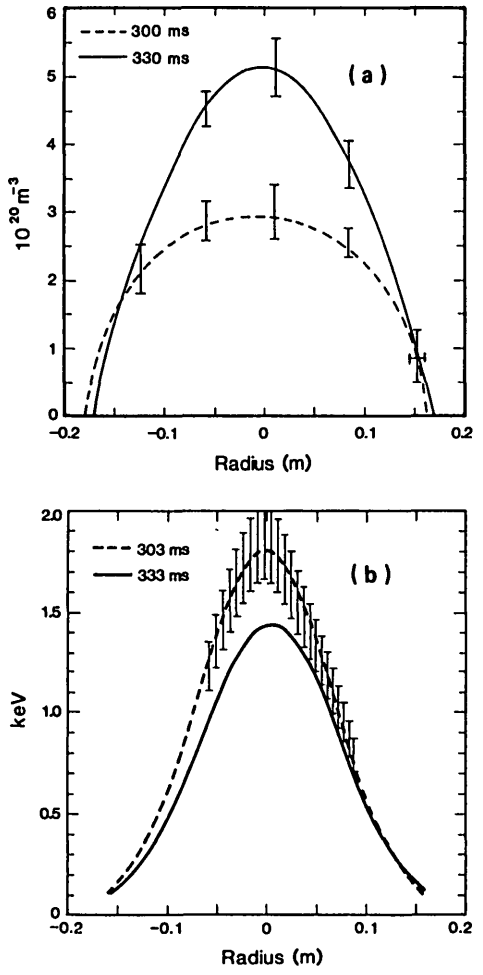

FIG.2. (a) Density profiles before and after pellet injection for the shot depicted in Fig.1, as determined by Abel inversion of data from a five-chord FIR interferometer. Typical error bars are shown at the locations of the interferometer chords.

(b) Electron temperature profiles as measured by second-harmonic ECE at approximately the same times as the density profile data. Error bars corresponding to the systematic uncertainty in calibration are shown for the upper trace.

as the line-average density decays somewhat more slowly, reaching a quasi-steady value of 3.0×10^{20} m^{-3} after 90–100 ms. The final density is greater than that of the target by about 25% in this case. For this example, both the neutron emission and the central ECE (second harmonic) show sawtoothing behaviour before and after pellet injection.

The shape of the electron temperature profile is essentially the same before and after injection, although the peak temperature is reduced in the post-injection plasma. The density profile, on the other hand, becomes significantly more peaked after injection, as shown in Fig.2, and relaxes slowly to a shape similar to that of the target gas-fuelled plasma. This behaviour may be seen more clearly in Fig.3, which depicts the temporal behaviour of the scalelengths a_{T_e}, the effective Gaussian width of the electron temperature profile, and r_n^{eff}, a measure of the density scalelength related to the 'peak-to-average ratio' and defined here by

$$r_n^{eff} = \int_0^a n(r)\, dr / n(0)$$

3. ANALYSIS TECHNIQUE

The data analysis is carried out using a modified version of the ONETWO [8] transport code. Parameterized profiles of $T_e(r)$ and $n_e(r)$, together with values of I_p, V_R, and the measured neutron rate, R_n^{exp}, are supplied at up to 20 instants (time-slices) before and after the time of pellet injection.

The physical processes considered in the analysis include electron and ion heat transport, particle transport, magnetic diffusion, neutral transport, and radiation. The analysis is performed in 1-D geometry,

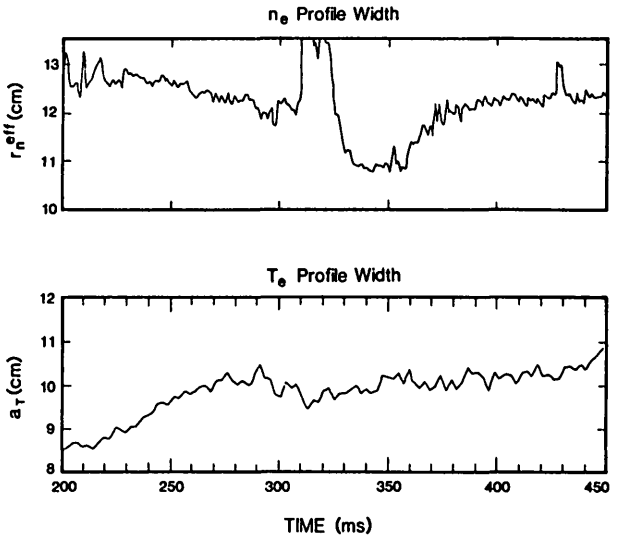

FIG.3. Evolution of density width and electron temperature width during the pellet injection shot depicted in Fig.1. The temperature profile is essentially unchanged by the pellet, while the density profile undergoes an initial transient, then peaks, and finally relaxes to its original shape.

assuming concentric circular flux surfaces. The relevant diffusion equations are:

$$\frac{\partial n_e}{\partial t} = -\nabla\cdot\Gamma_e + S_e \tag{1}$$

$$\frac{3}{2}\frac{\partial n_e T_e}{\partial t} = \frac{1}{r}\frac{\partial}{\partial r} r\left(n_e \chi_e \frac{\partial T_e}{\partial r} - \frac{5}{2} T_e \Gamma_e\right)$$

$$+ P_\Omega - P_\Delta - P_{rad} \tag{2}$$

$$\frac{3}{2}\frac{\partial\left(\sum_i n_i\right)T_i}{\partial t} = \frac{1}{r}\frac{\partial}{\partial r} r\left(\left(\sum_i n_i\right)\chi_i \frac{\partial T_i}{\partial r}\right.$$

$$\left. - \frac{5}{2} T_i\left(\sum_i \Gamma_i\right)\right) + P_\Delta - P_{CX} \tag{3}$$

$$\frac{\partial B_\theta}{\partial t} = \frac{\partial E}{\partial r} \tag{4}$$

Here, $\Gamma_{e,i}$ are the electron and ion particle fluxes; S_e is the net (electron) source rate from all processes; $\chi_{e,i}$ are the thermal diffusivities of electrons and ions, respectively; P_Ω is the Ohmic heating power density, $(E\cdot j)$; $P_\Delta = \frac{3}{2} n_e \sum_i \nu^E_{e,i}(T_e - T_i)$, with $\nu^E_{e,i} \propto n_i Z_i^2/m_i T_e^{3/2}$, is the electron–ion equilibration power; P_{rad} is the local radiated power density; and P_{CX} represents the charge-exchange loss term.

Boundary conditions for the electron temperature and density are taken from fits to the measured profiles. The ion temperature at the boundary is assumed to be equal to the local electron temperature. The boundary condition for the magnetic diffusion equation is obtained from the total plasma current.

A single impurity species, either carbon or oxygen, is assumed to be present, and the particle flux is taken to be ambipolar, i.e.

$$-\Gamma_e = \sum_i Z_i \Gamma_i \tag{5}$$

The impurity temperature is taken to be equal to that of the hydrogenic ion species. The total source rate (Eq.(1)) is obtained with the aid of a neutral transport package. An assumed global particle confinement time, τ_p^{in}, provides the necessary boundary condition for this calculation. For the plasma parameters considered here, the results of the analysis are insensitive to the choice of this parameter. Radiated power (Eq.(2)) is calculated for bremsstrahlung and line radiation due to the assumed impurity species.

For our purposes it is not necessary to model the internal particle source due to ablation of the pellet explicitly. Rather, an ad hoc source term S_{pel} is introduced which balances the observed $\partial n/\partial t$ at the time of injection. This technique avoids numerical difficulties associated with the very rapid flows immediately after injection.

The magnetic diffusion equation is solved assuming classical resistivity and using $I_p(t)$ as the boundary condition. Z_{eff} is adjusted so as to match the experimental loop voltage, and the resulting value is compared with that determined by the visible bremsstrahlung diagnostic for consistency. The shape of the Z_{eff} profile is adjusted over a narrow range to provide consistency between the computed value of the axial safety factor q_0 and the presence or absence of sawteeth in the discharge. Since the experimental inputs are averaged over sawtooth periods, no explicit effects of internal disruptions are included in the time-dependent analysis. The time-averaged effects of sawteeth on the central energy and particle balance are therefore included in the inferred values of the transport coefficients. Simple estimates based on the observed sawtooth amplitude and period indicate that sawtooth activity dominates the power balance inside the $q = 1$ surface, which for these discharges corresponds to about the central one-quarter of the minor radius.

Since the ion temperature profile is not measured for these experiments, it is not possible to uniquely determine the local ion thermal diffusivity $\chi_i(r, t)$. Instead, the ion heat transport equation is solved assuming an ion thermal diffusivity of the form

$$\chi_i(r,t) = W(t) \times \chi_i^{Neo} + D_b f(q)$$

where $\chi_i^{Neo}(r, t)$ is the Chang–Hinton neoclassical coefficient, D_b is the Bohm diffusivity and

$$f(q) = 1 - \frac{1}{1+(1/q-1)^2} \quad q \leqslant 1$$

$$= 0 \qquad\qquad q > 1$$

models the time-averaged effect of sawtooth activity. The time-dependent anomaly factor $W(t)$ is dynamically adjusted so as to reproduce the observed neutron emission rate, which depends primarily on the central

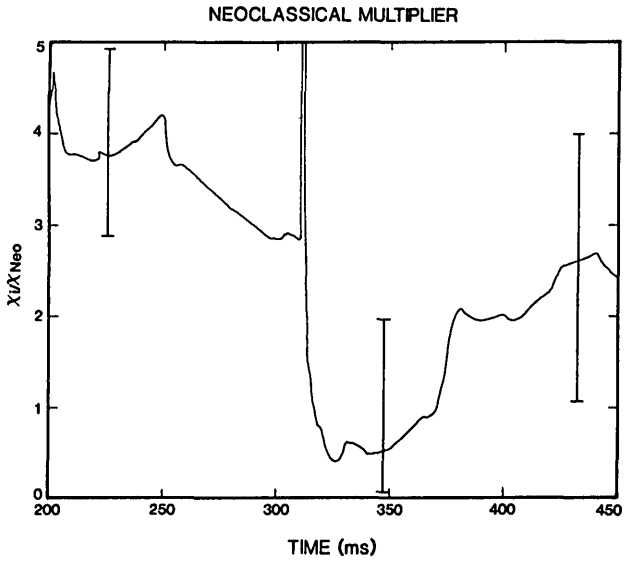

FIG.4. Evolution of the anomaly factor with respect to neoclassical ion conduction inferred by the transport code for the shot depicted in Figs 1–3. Error bars are estimated by a procedure described in Section 5.

ion temperature, $T_i(0)$, and, more weakly, on the ion temperature profile width. A 'feedback' procedure

$$\frac{dW}{dt} = G_1 \left(\frac{R_n^{exp} - R_n^{code}}{R_n^{exp}} \right) + G_2 \frac{d}{dt} \left(\frac{R_n^{exp} - R_n^{code}}{R_n^{exp}} \right)$$

is used to determine W(t). Here R_n^{exp} is the experimentally observed neutron rate, R_n^{code} is the rate predicted by the code, and the gains G_1 and G_2 are chosen to avoid numerical instability. A similar procedure is used to adjust Z_{eff} to obtain the correct voltage when solving the magnetic diffusion equation.

4. RESULTS

Pre-pellet plasmas typically exhibit values of ion thermal conductivity which are a factor of three to five higher than neoclassical. This trend is apparent over a wide range of parameters and confirms earlier work [2–4] which concluded that significant anomalous ion losses were present. Following pellet injection, the anomaly factor typically decreases to order unity, as shown in the time history in Fig.4. In this example, the improvement persists for about 60 ms, following which a significant anomaly reappears. The inferred value of χ_i at the half-radius falls from about 0.5 $m^2 \cdot s^{-1}$ before pellet injection to less than 0.1 $m^2 \cdot s^{-1}$ at 50 ms after pellet injection. The variation of the ion thermal diffusivity before and after pellet injection for a range of plasma currents is shown in Fig.5. The improvement is consistent and persists for between 20 ms and > 100 ms in different discharges.

While ion thermal transport decreases after pellet injection, the electron thermal conductivity κ_e in general either remains constant or increases somewhat according to the code results. However, the increase in these cases may be artificial, since the radiation losses included in these code runs are the result of a calculation based on a single, low-Z impurity species rather than on bolometric measurements. With this assumption, the code predicts that the radiated power in the central two-third of the discharge should account for less than 15% of the Ohmic input power, while in roughly similar discharges for which bolometric measurements are available, P_{rad} is found [9] to vary between 15% and 35% of the Ohmic power, with values as high as 50% observed shortly after pellet injection in some cases. It is therefore possible that increased radiation loss at the higher density following injection is being incorrectly attributed to electron thermal conduction. The uncertainties are thus more severe for electron transport than for ion transport. Values of the electron thermal conductivity corresponding to the ion data of Fig.5 are shown in Fig.6. From neo-Alcator scaling we would expect κ_e to be independent of density and therefore unchanged after pellet injection. If the increases shown are not due to errors in modelling, they may result from an unfavourable

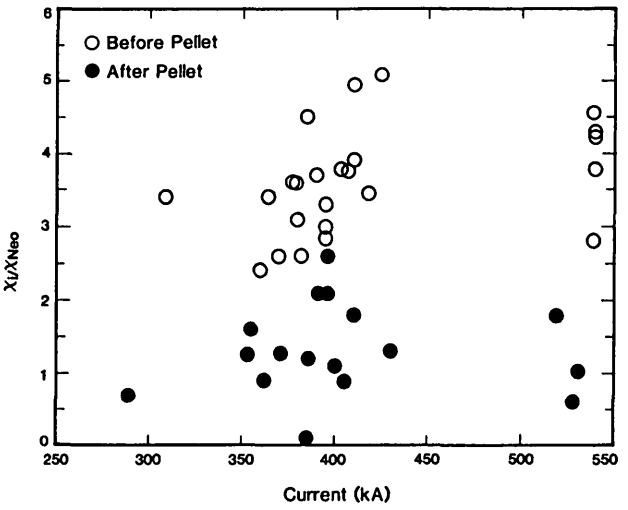

FIG.5. Inferred value of the ion thermal conduction anomaly before and after pellet injection for several plasma currents. The post-pellet values are taken 30–50 ms after injection.

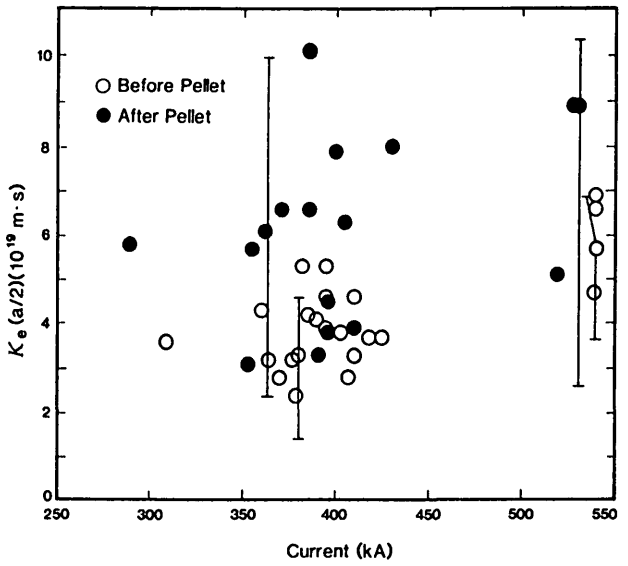

FIG.6. Electron thermal conductivity evaluated at the half-radius before and after injection. The calculation of κ_e is subject to uncertainties in the radiated power term which are included in the typical error bars shown.

dependence on ∇n, which might be expected for drift-wave transport. However, because of the uncertainty noted above, no strong conclusions on this point can be drawn from the present data, beyond the qualitative observation that, in contrast to ion losses, electron losses do not in general decrease following pellet injection.

The most apparent difference between the pellet-fuelled and the gas-fuelled discharges in terms of directly measured experimental quantities is the more peaked density profiles typical of the post-injection plasmas. We note that the temporal behaviour of the ion anomaly depicted in Fig.4 is similar to the evolution of the density profile width r_n^{eff} for this shot (Fig.3). Figure 7 is a plot of these quantities for a different shot, in which the peaking of the density profile persists for several hundred milliseconds. The qualitative similarity of the two traces is also evident in this case, suggesting a correlation between the shape of the density profile and the mechanism for the anomalous ion loss. A plot of χ_i/χ_{Neo} versus r_n^{eff} for a collection of data is shown in Fig.8 and does indicate at least a weak correlation. However, the large scatter in the data may imply that the 'proper' scaling variable for the ion anomaly is more complicated than the simple global quantity r_n^{eff}. The fact that several of the points in Fig.8 correspond to anomaly factors less than one is consistent with the estimated errors discussed in the following section.

5. ERROR SENSITIVITY

Since the difference between T_e and T_i is small, particularly after pellet injection, there are necessarily significant uncertainties in the values of the transport coefficients resulting from our analysis. We have conducted sensitivity studies to assess the reliability of our results.

The principal experimental uncertainties arise from the accuracy of the measurement of T_e and the density profile. From a comparison of calibrations with soft-X-ray and Thomson scattering techniques and from shot-to-shot variation over similar discharges, the error in the central electron temperature is estimated to be of the order of 10%. The width of the T_e profile is typically measured to similar accuracy. The error in the line integral of the density as measured by the sub-millimetre interferometer is less than ±5% for densities in the range $1 \times 10^{20} \leqslant \bar{n} \leqslant 3 \times 10^{20}\,m^{-3}$. However, the Abel transform required to obtain local $n_e(r)$ introduces errors, and the approximation by a three-parameter standard profile used in the code further degrades the accuracy. We estimate a 15% error bar on $n_e(0)$ to be reasonable. This estimate is supported by a comparison with Thomson scattering data. The error in the calibration of the absolute neutron rate is less than 25%, which has little impact on the implied ion temperature.

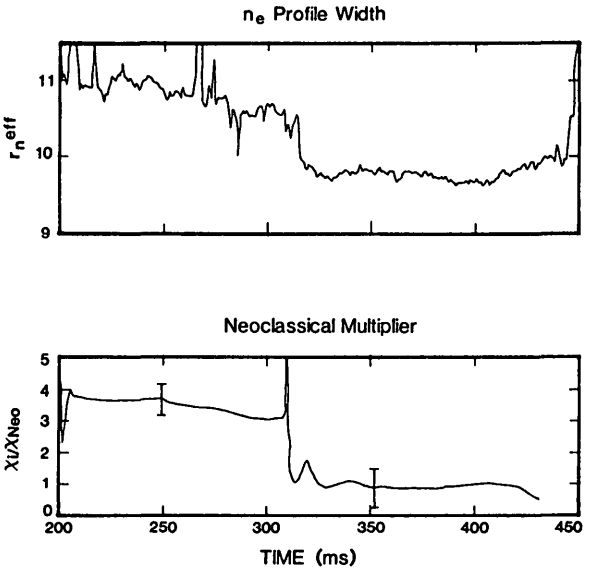

FIG.7. Evolution of the density profile width and ion thermal conduction anomaly for a shot with no sawtooth activity following injection.

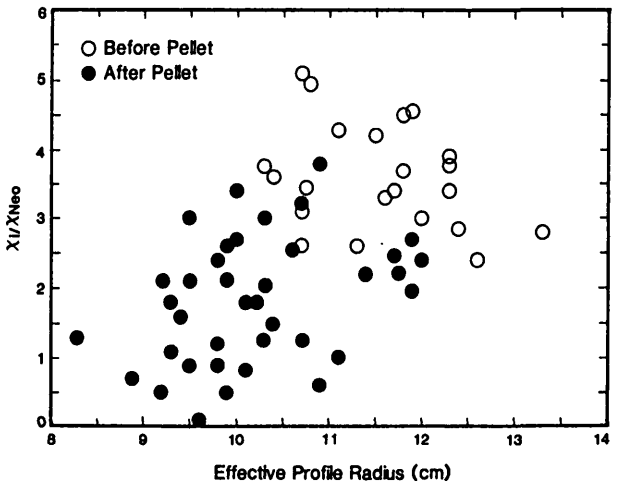

FIG.8. Ion thermal conduction anomaly as a function of density profile width. Post-pellet values include data up to 200 ms following injection.

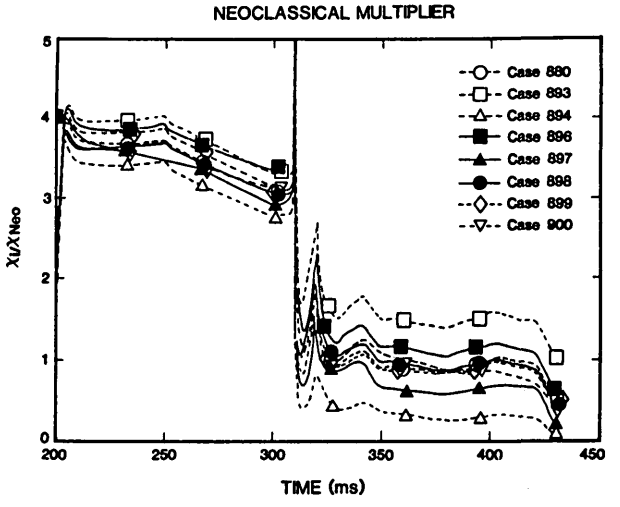

FIG.9. Results of a series of code runs based on the same shot as Fig.7, but with parameters varied within limits of experimental error. The most extreme cases (labelled 893 and 894) correspond to variation of the electron temperature by ±10%. The case labelled 900 was run using a false density profile with an effective width which behaved similar to that in Fig.3 as a function of time. The result is essentially indistinguishable from the nominal case (880).

The effects of varying parameters within these error estimates on the evaluation of the neoclassical multiplier are shown in Fig.9. Each trace represents a code run based on the shot depicted in Fig.7, but with different input values corresponding to assumed errors in calibration or profile determination. The pre-pellet discharge is clearly inconsistent with neoclassical ion transport in all cases, while the post-injection values are all below $\chi_i/\chi_{Neo} = 1.5$. Some of the runs lead to anomaly factors less than unity after injection. The relatively larger spread in the post-pellet traces is, of course, due to the closer coupling between electrons and ions and the reduction in $(T_e - T_i)$.

In the above, errors in calibration have been assumed to be consistent throughout the discharge. In the case of the density profile, particularly, it is also important to consider the effect of possible time-dependent errors on the analysis. This is especially true in view of the apparent correlation between the evolution of the density profile and the anomalous transport illustrated in Figs 3, 4 and 7. The possibility that this correlation could be an artefact of the analysis technique was tested by re-doing the analysis of the data of Fig.7 using a false $n_e(r, t)$ profile such that $\bar{n}_e(t)$ was unchanged, but the time history of $r_n^{eff}(t)$ after injection more closely resembled that of Fig.3, i.e. first decreasing and then returning close to its pre-pellet value. The resulting behaviour of the inferred anomaly factor for this case is included in Fig.9 and is essentially indistinguishable from the nominal value. We may therefore conclude that the relationship between density profile and ion transport is valid and is not a consequence of implicit dependences inherent in the analysis.

6. DISCUSSION

It is apparent from the data that the gas-fuelled plasmas exhibit significant anomalies in ion thermal diffusivity which are reduced after pellet injection. Furthermore, the effect appears to be related to the peaking of the density profile, although the 'effective profile width' r_n^{eff} may not be the best scaling parameter when applied to a range of discharges. In particular, we note that the gas-fuelled cases in Fig.8 show no positive correlation with profile width. Nevertheless, we are led to consider anomalous transport mechanisms which depend directly or indirectly on the density profile.

In applying the results of our analysis to any such mechanism, it is necessary to consider several points. First, in the absence of measured profiles for the ion temperature, the analyses have been carried out under the assumption that the anomalous ion conduction is of the form of a constant multiplier times the neoclassical coefficient. There is, of course, no valid basis for such a model, and specific anomalous transport

models may in fact scale quite differently. The self-consistent $T_i(r, t)$ generated by the code will therefore not correspond to that resulting from an alternative model with the same 'average' effects. This fact is important for mechanisms which depend on the ion temperature profile, for example. Further, the values of χ_i at particular locations cannot be directly compared with theoretical predictions with different spatial dependences. Another difficulty arises from the reduction of experimental data to simplified analytic forms for use in the code. While the parameterization is adequate for the calculation described, as evidenced by the relative insensitivity of the results to artificial variations in the profiles, it is not sufficiently detailed to give accurate values for gradients, for example. Use of these forms in conjunction with models which depend on local scalelengths, for instance of the density and temperature, may produce unreliable results.

Keeping these considerations in mind, we nevertheless may examine our data in the context of some specific mechanisms, looking for general trends rather than precise agreement. One possible effect which bears at least qualitative similarities to the experimental results is transport arising from ∇T_i-driven ion drift instabilities (e.g. the ion mixing mode) [10]. Here the relevant parameter is the quantity

$$\eta_i = \frac{d \ln T_i}{d \ln n_i}$$

the ratio of the ion density and temperature scalelengths. The mode is unstable for large values of η_i and can theoretically lead to anomalous ion heat loss. An approximate form [10] for the critical value for stability in the collisionless limit is

$$\eta_{crit} \approx \frac{1}{2}\left[1 + \left(1 + 113\left(\frac{r_n}{Rq}\right)^2\right)^{1/2}\right]$$

where $r_n = (d \ln n/dr)^{-1}$ is the local density scalelength and should not be confused with r_n^{eff} defined in Section 2. The values of η_i derived from our analysis are typically found to decrease after pellet injection, as the steepening of the measured density profile is only partially compensated by an increase in the gradient of the inferred ion temperature profile. While there is no correlation between χ_i/χ_i^{Neo} and the ratio η_i/η_{crit}, as shown in Fig.10, it is interesting that the values of η_i/η_{crit} for both pellet-fuelled and gas-fuelled cases lie close to unity, easily within the combination of experimental and modelling errors and theoretical uncertainty. While this result may be purely coincidental, it might be conjectured that the thermal transport due to these modes has the effect of flattening the ion temperature profile sufficiently to reduce η_i to the marginally stable value; effective saturation of the mode would therefore occur at an amplitude corresponding to the self-consistent enhancement of χ_i. Simulations based on the estimated thermal diffusivity contained in Ref.[10] indicate that the transport is sufficiently large to produce this result, while simulations with only neoclassical ion transport lead to more peaked ion temperature profiles and therefore larger values of η_i such that $\eta_i \gg \eta_{crit}$ over much of the plasma for the pre-injection case. On the other hand, more recent theoretical work [11, 12] on the non-linear saturation of the mixing mode may lead to smaller values of the saturated amplitude and the corresponding anomalous transport.

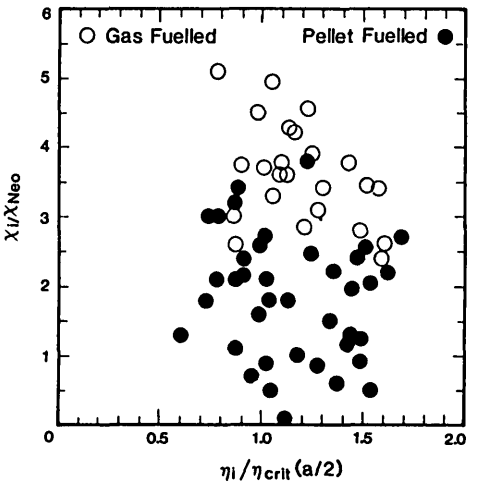

FIG.10. Ion thermal conduction anomaly as a function of the ratio η_i/η_{crit} evaluated at the half-radius, using ion temperature profiles obtained from the code results.

While the clearest difference between gas-fuelled and pellet-fuelled discharges is their density profiles, they are not identical in all other respects and we cannot rule out other causes for the improved ion confinement. For example, the lack of intense gas puffing in pellet discharges may change the power balance in the discharge edge. Further, the differences in the density profiles reflect differences in particle transport and, while we can recognize correlations between energy and particle transport, cause and effect are more difficult to sort out.

7. CONCLUSIONS

We have confirmed the presence of significant excess ion thermal losses in gas-fuelled Ohmic discharges in the density range $10^{20} \leqslant \bar{n}_e \leqslant 3 \times 10^{20}\ m^{-3}$ and with currents $250 \leqslant I_p \leqslant 550$ kA. The ion heat flux corresponds to a thermal diffusion coefficient three to five times the Chang-Hinton neoclassical value. Following pellet injection, the ion thermal diffusivity at the half-radius decreases from values near $0.5\ m^2 \cdot s^{-1}$ to values near $0.1\ m^2 \cdot s^{-1}$; the latter correspond to neoclassical predictions for these plasma parameters. While in these cases the ion thermal conductivity κ_i typically falls, the electron thermal conductivity κ_e appears to rise or to remain roughly constant.

In some instances the neoclassical level of ion transport persists throughout the remainder of the discharge. More typically, the ratio of χ_i/χ_i^{Neo} increases with time and may approach the pre-injection value. The behaviour of the anomaly factor for a given discharge is strongly correlated with the peaking of the density profile, and some correlation between the global parameter r_n^{eff} and the anomalous diffusivity is apparent from the data. The values of η_i obtained are close to the critical values for marginal stability for the ion mixing mode. One may speculate that the large spread in ion thermal conductivity observed corresponds to the thermal conductivity required to sufficiently flatten the ion temperature profile so as to provide stability with respect to a given density profile.

The typical magnitude of the anomalous ion transport in the gas-fuelled target plasmas in this parameter range corresponds to $\chi_i^{anom} \approx 0.4\ m^2 \cdot s^{-1}$. The presence of an anomalous thermal diffusivity of this magnitude in higher-density discharges would be sufficient to account for the observed saturation in global energy confinement in gas-fuelled Alcator C plasmas. Moreover, the lack of saturation in the best high-density pellet-fuelled cases, which also exhibited the strongest peaking of the density profile, is consistent with the effect documented here. Therefore, while the present work cannot unambiguously account for the high-density results, it suggests that a similar mechanism is responsible.

ACKNOWLEDGEMENTS

The authors wish to thank the Alcator C operating team and technical staff for their invaluable contributions to this work. They are also grateful to R. Englade and P. Diamond for helpful discussions regarding the ion mixing mode. This work was supported by the United States Department of Energy, Contract No. DE-AC02-78ET-51013.

REFERENCES

[1] GREENWALD, M., GWINN, D., MILORA, S., PARKER, J., PARKER, R., et al., Phys. Rev. Lett. **53** (1984) 352.
[2] PARKER, R.R., Bull. Am. Phys. Soc. **27** (1982) 986; ALCATOR GROUP, ALCATOR C Status and Program Plan, Massachusetts Inst. of Tech., Cambridge, Rep. PFC/IR-82-3 (Dec. 1982).
[3] BLACKWELL, B., FIORE, C.L., GANDY, R., GONDHALEKAR, A., GRANETZ, R.S., et al., in Plasma Physics and Controlled Nuclear Fusion Research 1982 (Proc. 9th Int. Conf. Baltimore, 1982), Vol.2, IAEA, Vienna (1983) 27.
[4] PARKER, R.R., GREENWALD, M., LUCKHARDT, S.C., MARMAR, E.S., PORKOLAB, M., WOLFE, S.M., Nucl. Fusion **25** (1985) 1127.
[5] CHANG, C.S., HINTON, F.L., Phys. Fluids **25** (1982) 1493.
[6] GOLDSTON, R.J., Plasma Phys. Controll. Fusion **26**, 1A (1984) 87 (Invited Papers of 11th Europ. Conf. Aachen, 1983).
[7] MILORA, S.L., J. Fusion Energy **1** (1981) 15.
[8] PFEIFFER, W.W., DAVIDSON, R.H., MILLER, R.L., WALTZ, R.E., ONETWO: A Computer Code for Modelling Plasma Transport in Tokamaks, Gulf General Atomic, Inc., San Diego, CA, Rep., GA-A16178 (1980).
[9] KNOWLTON, S., personal communication (1985).
[10] ANTONSEN, T., COPPI, B., ENGLADE, R., Nucl. Fusion **19** (1979) 641.
[11] LEE, G.S., DIAMOND, P.H., in Sherwood Annual Controlled Fusion Theory Conference (Proc. Mtg Madison, WI, 1985) (1985) paper 1S24.
[12] ENGLADE, R., COPPI, B., MIGIUOLO, S., ibid., paper 2Q20.

(Manuscript received 16 September 1985
Final manuscript received 5 December 1985)